Inorg. Chem. **2004**, *43*, 931–944

Coordination Polymers Assembled from Angular Dipyridyl Ligands and Cu^{II}, Cd^{II}, Co^{II} Salts: Crystal Structures and Properties

Zheng Huang, Hai-Bin Song, Miao Du, Shen-Tan Chen, and Xian-He Bu*

Department of Chemistry, Nankai University, Tianjin 300071, P. R. China

Joan Ribas

Departament de Química Inorgànica, Universitat de Barcelona, Diagonal, 647, 08028-Barcelona, Spain

Received August 24, 2003

Six new metal-organic coordination networks based on linking unit 2,5-bis(4-pyridyl)-1,3,4-thiadiazole (**L**^{1}) or 2,5-bis(3-pyridyl)-1,3,4-oxadiazole (**L**^{3}) and inorganic Cu^{II}, Cd^{II}, and Co^{II} salts have been prepared and structurally characterized by single-crystal X-ray analysis. Using **L**^{1} to react with three different Cu^{II} salts, $Cu(OAc)_2 \cdot H_2O$, $Cu(NO_3)_2 \cdot 3H_2O$, and $CuSO_4 \cdot 5H_2O$, respectively, two different one-dimensional (1-D) coordination polymers, $\{[Cu_2\mathbf{L}^{1}(\mu\text{-}OAc)_4](CHCl_3)_2\}_n$ (**1**) [triclinic, space group $P\bar{1}$, $a = 7.416(3)$ Å, $b = 8.207(3)$ Å, $c = 14.137(5)$ Å, $\alpha = 100.333(7)°$, $\beta = 105.013(6)°$, $\gamma = 94.547(6)°$, $Z = 1$] and $\{[Cu\mathbf{L}^{1}(NO_3)_2](CHCl_3)_{0.5}\}_n$ (**2**) [monoclinic, space group $C2/c$, $a = 28.070(8)$ Å, $b = 9.289(3)$ Å, $c = 15.235(4)$ Å, $\beta = 113.537(5)°$, $Z = 8$], and a *chiral* 3-D open framework, $\{[Cu\mathbf{L}^{1}(H_2O)(SO_4)](H_2O)_2\}_n$ (**3**) [orthorhombic, space group $P2_12_12_1$, $a = 5.509(2)$ Å, $b = 10.545(4)$ Å, $c = 29.399(11)$ Å, $Z = 4$], were obtained. Reaction of **L**^{1} and $Cd(ClO_4)_2 \cdot 6H_2O$ or $Co(ClO_4)_2 \cdot 6H_2O$, in the presence of NH_4SCN, yielded another 3-D open framework, $\{[Cd\mathbf{L}^{1}(NCS)_2](CH_3OH)_{1.5}\}_n$ (**4**) [monoclinic, space group $C2/c$, $a = 28.408(10)$ Å, $b = 9.997(5)$ Å, $c = 7.358(4)$ Å, $\beta = 99.013(8)°$, $Z = 4$], or a 2-D network, $\{[Co(\mathbf{L}^{1})_2(NCS)_2]\text{-}(H_2O)_{2.5}\}_n$ (**5**) [orthorhombic, space group $Pnna$, $a = 22.210(5)$ Å, $b = 12.899(3)$ Å, $c = 20.232(4)$ Å, $Z = 4$]. When **L**^{1} was replaced by **L**^{3} to react with $Co(ClO_4)_2 \cdot 6H_2O$ and NH_4SCN, another 2-D coordination polymer, $[Co(\mathbf{L}^{3})_2(NCS)_2]_n$ (**6**) [monoclinic, space group $P2_1/c$, $a = 8.120(3)$ Å, $b = 9.829(4)$ Å, $c = 17.453(6)$ Å, $\beta = 103.307(6)°$, $Z = 2$], was constructed. These results indicate that the nature of the ligands, metal centers, or counteranions plays the critical role in construction of these novel coordination polymers. The interesting porous natures of two 3-D open frameworks **3** and **4** were investigated by TGA and XPRD techniques, and the magnetic properties of the Cu^{II} and Co^{II} complexes were studied by variable-temperature magnetic susceptibility and magnetization measurements.

Introduction

The crystal engineering of one-, two-, or three-dimensional coordination polymers has attracted considerable current attention, not only because of their novel topologies and fascinating structural diversities,[1] but also for their potential applications in optical, electrical, magnetic, and microporous materials.[2] The ultimate aim of supramolecular chemistry is to control the structure of the target product with tailored properties and functions, for which much effort has been devoted to the attempts at designing and constructing new coordination polymers with specific network topologies, and

* Corresponding author. E-mail: buxh@nankai.edu.cn. Fax: +86-22-23502458. Phone: +86-22-23502809.

(1) For examples: (a) Batten, S. R.; Robson, R. *Angew. Chem., Int. Ed.* **1998**, *37*, 1460. (b) Blake, A. J.; Champness, N. R.; Hubberstey, P.; Li, W.-S.; Withersby, M. A.; Schröder, M. *Coord. Chem. Rev.* **1999**, *183*, 117. (c) Hagrman, P. J.; Hagrman, D.; Zubieta, J. *Angew. Chem., Int. Ed.* **1999**, *38*, 2639. (d) Moulton, B.; Zaworotko, M. J. *Chem. Rev.* **2001**, *101*, 1629.

(2) For examples: (a) Fujita, M.; Kwon, Y. J.; Washizu, S.; Ogura, K. *J. Am. Chem. Soc.* **1994**, *116*, 1151. (b) Venkataraman, D.; Moore, J. S.; Lee, S. *Nature* **1995**, *374*, 792. (c) Xiong, R.-G.; You, X.-Z.; Abrahams, B. F.; Xue, Z.; Che, C.-M. *Angew. Chem., Int. Ed.* **2001**, *40*, 4422. (d) Evans, O. R.; Lin, W. *Acc. Chem. Res.* **2002**, *35*, 511 and references therein. (e) Rosi, N. L.; Eckert, J.; Eddaoudi, M.; Vodak, D. T.; Kim, J.; O'Keeffe, M.; Yaghi, O. M. *Science* **2003**, *300*, 1127. (f) Galán-Mascarós, J. R.; Dunbar, K. R. *Angew. Chem., Int. Ed.* **2003**, *42*, 2289.

10.1021/ic034999d CCC: $27.50
Published on Web 12/31/2003

Chart 1

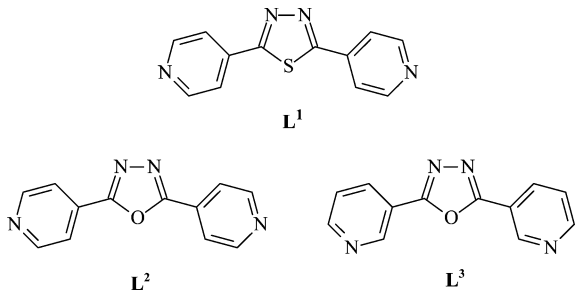

trying to investigate the relationship between the structures and physicochemical properties. The synthetic strategies for these polymers come from a variety of parameters, basically including the versatile coordination geometries of metal nodes, and the design of suitable organic ligands. So far, a variety of discrete and a wide range of one- or multidimensional infinite solid-state coordination architectures have been achieved by chemists in the past decade.[1,3]

We and others have been currently investigating the coordination chemistry of an angular dipyridyl-donor ligand, 2,5-bis(4-pyridyl)-1,3,4-oxadiazole (**L²**), and its 3-*N*-donor analogue 2,5-bis(3-pyridyl)-1,3,4-oxadiazole (**L³**) (see Chart 1).[4a−h] Such ligands exhibit several particular characteristics when bonding to the metal centers: (a) As reported in our previous work, these ligands can take versatile bonding modes, such as monodentate (using one pyridyl nitrogen donor), bidentate bridging (using two pyridyl nitrogen donors), and tridentate bridging (using two pyridyl and one oxadiazole nitrogen donors) coordination fashions in different conditions. (b) The structural geometries of the ligands themselves are also multiform. The dihedral angles between the oxadiazole ring and two pyridyl rings as well as that between two pyridyl rings within each ligand are changeful and adaptable to meet the requirements for constructing diverse frameworks, and so is the angle between the central oxadiazole ring and two pyridyl nitrogen donors. With respect to **L³**, it can exhibit three *trans* or *cis* conformations under approximate conditions. (c) The aromatic groups within each ligand, including two pyridyl rings and the central oxadiazole system, sometimes show a tendency to completely or partly participate in intermolecular $\pi-\pi$ interactions, which may affect the packing arrangement of the crystal structures. Recently, the role of anions in the construction of novel Ag^{I} coordination polymers with a related ligand, 2,5-bis(4-pyridyl)-1,3,4-thiadiazole (**L¹**, Chart 1), was initially investigated by us, and some different structural features were observed in these complexes compared with the corresponding Ag−**L²** supramolecular systems.[4i] As a continuation of our systemic contribution on this interesting project, we describe here the preparation and structural characterization of a series of new Cu^{II}, Cd^{II}, and Co^{II} coordination polymers with **L¹** and **L³**, including $\{[Cu_2\mathbf{L^1}(\mu\text{-OAc})_4](CHCl_3)_2\}_n$ (**1**), $\{[Cu\mathbf{L^1}(NO_3)_2](CHCl_3)_{0.5}\}_n$ (**2**), $\{[Cu\mathbf{L^1}(H_2O)(SO_4)](H_2O)_2\}_n$ (**3**), $\{[Cd\mathbf{L^1}(NCS)_2](CH_3OH)_{1.5}\}_n$ (**4**), $\{[Co\mathbf{L^1}_2(NCS)_2](H_2O)_{2.5}\}_n$ (**5**), and $[Co\mathbf{L^3}_2(NCS)_2]_n$ (**6**). Thermogravimetric analysis (TGA) and X-ray powder diffraction (XRPD) techniques were utilized to study the porous natures of materials **3** and **4**. The magnetic properties of the Cu^{II} and Co^{II} complexes were investigated and the magneto-structural correlation also discussed in detail.

Experimental Section

Materials and General Methods. All the solvents and reagents for synthesis were commercially available and used as received. The ligand **L¹** was commercially available and used without further purification, and **L³** was synthesized according to the literature procedure.[5] Fourier transform (FT) IR spectra (KBr pellets) were taken on a FT-IR 170SX (Nicolet) spectrometer. Carbon, hydrogen, and nitrogen analyses were performed on a Perkin-Elmer 240C analyzer. Thermogravimetric analysis (TGA) experiment was carried out on a Dupont thermal analyzer from room temperature to 800 °C under nitrogen atmosphere at a heating rate of 10 °C/min. X-ray powder diffraction (XRPD) data were recorded on a Rigaku RU200 diffractometer at 60 kV, 300 mA for Cu Kα radiation ($\lambda = 1.5406$ Å), with a scan speed of 2 deg/min and a step size of 0.02° in 2θ. The calculated XRPD pattern was produced using the SHELXTL-XPOW program and single-crystal reflection data.

Magnetic Studies. The variable-temperature magnetic susceptibilities were measured in "Servei de Magnetoquímica (Universitat de Barcelona)" on polycrystalline samples (ca. 30 mg) with a Quantum Design MPMS SQUID susceptometer operating at a magnetic field of 0.1 T between 2 and 300 K. The diamagnetic corrections were evaluated from Pascal's constants for all the constituent atoms. Magnetization measurements were carried out at low temperature (2 K) in 0−5 T range.

Synthesis of $\{[Cu_2\mathbf{L^1}(\mu\text{-OAc})_4](CHCl_3)_2\}_n$, 1. A solution of $Cu(OAC)_2{\cdot}H_2O$ (39 mg, 0.2 mmol) in CH_3OH (10 mL) was carefully layered on a solution of **L¹** (24 mg, 0.1 mmol) in $CHCl_3$ (15 mL) in a straight glass tube. After ca. two weeks, bluish-green single crystals were obtained. Yield: 46 mg (55%). Anal. Calcd for $\{[Cu_2\mathbf{L^1}(\mu\text{-OAc})_4](CHCl_3)_2\}_n$: C, 31.37; H, 2.63; N, 6.65%. Found: C, 31.33; H, 3.01; N, 7.02%. IR (KBr, cm^{-1}): 3018w, 2935w, 1616vs, 1606vs, 1430vs, 1346w, 1220w, 1209w, 1091w, 999w, 833w, 750m, 700m, 683m, 666w, 627w, 611w, 491w.

(3) For examples: (a) Fujita, M.; Kwon, Y. J.; Sasaki, O.; Yamaguchi, K.; Ogura, K. *J. Am. Chem. Soc.* **1995**, *117*, 7278. (b) Stang, P. J.; Zhdankin, V. V. *Chem. Rev.* **1996**, *96*, 1123. (c) Withersby, M. A.; Blake, A. J.; Champness, N. R.; Hubberstey, P.; Li, W.-S.; Schröder, M. *Angew. Chem., Int. Ed. Engl.* **1997**, *36*, 2327. (d) Fujita, M. *Chem. Soc. Rev.* **1998**, *27*, 417. (e) Carlucci, L.; Ciani, G.; Macchi, P.; Proserpio, D. M. *Chem. Commun.* **1998**, 1837. (f) Carlucci, L.; Cozzi, N.; Ciani, G.; Moret, M.; Proserpio, D. M.; Rizzato, S. *Chem. Commun.* **2002**, 1354. (g) Noro, S.; Kitaura, R.; Kondo, M.; Kitagawa, S.; Ishii, T.; Matsuzaka, H.; Yamashita, M. *J. Am. Chem. Soc.* **2002**, *124*, 2568.

(4) (a) Du, M.; Bu, X.-H.; Guo, Y.-M.; Liu, H.; Batten, S. R.; Ribas, J.; Mak, T. C. W. *Inorg. Chem.* **2002**, *41*, 4904. (b) Du, M.; Chen, S.-T.; Bu, X.-H. *Cryst. Growth Des.* **2002**, *2*, 625. (c) Du, M.; Liu, H.; Bu, X.-H. *J. Chem. Crystallogr.* **2002**, *32*, 57. (d) Fang, Y.-Y.; Liu, H.; Du, M.; Guo, Y.-M.; Bu, X.-H. *J. Mol. Struct.* **2002**, *608*, 229. (e) Du, M.; Bu, X.-H.; Huang, Z.; Chen, S.-T.; Guo, Y.-M.; Diaz, C.; Ribas, J. *Inorg. Chem.* **2003**, *42*, 552. (f) Dong, Y.-B.; Ma, J.-P.; Huang, R.-Q.; Liang, F.-Z.; Smith, M. D. *J. Chem. Soc., Dalton Trans.* **2003**, 1472. (g) Dong, Y.-B.; Cheng, J.-Y.; Wang, H.-Y.; Huang, R.-Q.; Tang, B.; Smith, M. D.; Loye, H.-C. *Chem. Mater.* **2003**, *15*, 2593 and references therein. (h) Du, M.; Guo, Y.-M.; Chen, S.-T.; Bu, X.-H.; Batten, S. R.; Ribas, J. *Inorg. Chem.*, in press. (i) Huang, Z.; Du, M.; Song, H.-B.; Bu, X.-H. *Cryst. Growth Des.* **2004**, in press (DOI: 10.1021/cg0341095).

(5) Bentiss, F.; Lagrenee, M. *J. Heterocycl. Chem.* **1999**, *36*, 1029.

Table 1. Crystal Data and Structure Refinement Parameters for Complexes **1**−**6**

	1	**2**	**3**[c]	**4**	**5**	**6**
chemical formula	$C_{22}H_{22}Cl_6Cu_2N_4O_8S$	$C_{12.5}H_{8.5}Cl_{1.5}CuN_6O_6S$	$C_{12}H_{14}CuN_4O_7S_2$	$C_{15.5}H_{14}CdN_6O_{1.5}S_3$	$C_{26}H_{21}CoN_{10}O_{2.5}S_4$	$C_{26}H_{16}CoN_{10}O_2S_2$
fw	842.28	487.53	453.93	516.91	700.70	623.54
space group	$P\bar{1}$	$C2/c$	$P2_12_12_1$	$C2/c$	$Pnna$	$P2_1/c$
a (Å)	7.416(3)	28.070(8)	5.509(2)	28.408(10)	22.210(5)	8.120(3)
b (Å)	8.207(3)	9.289(3)	10.545(4)	9.997(5)	12.899(3)	9.829(4)
c (Å)	14.137(5)	15.235(4)	29.399(11)	7.358(4)	20.232(4)	17.453(6)
α/deg	100.333(7)	90	90	90	90	90
β/deg	105.013(6)	113.537(5)	90	99.013(8)	90	103.307(6)
γ/deg	94.547(6)	90	90	90	90	90
V/Å^3	810.4(5)	3641.9(17)	1707.8(11)	2063.9(15)	5796(2)	1355.6(9)
Z	1	8	4	4	4	2
D/g cm^{-3}	1.726	1.778	1.765	1.664	0.803	1.528
μ/mm^{-1}	1.921	1.580	1.568	1.382	0.464	0.833
T/K	293(2)	293(2)	293(2)	293(2)	293(2)	293(2)
$R^a/R_w{}^b$	0.0528/0.1413	0.0420/0.1101	0.0374/0.1172	0.0299/0.0973	0.0693/0.2145	0.0475/0.0920

[a] $R = \sum||F_o| - |F_c||/\sum|F_o|$. [b] $R_w = [\sum[w(F_o^2 - F_c^2)^2]/\sum w(F_o^2)^2]^{1/2}$. [c] Flack parameter = 0.03(2).

Synthesis of {[CuL^1(NO$_3$)$_2$](CHCl$_3$)$_{0.5}$}$_n$, 2. The same synthetic procedure as for **1** was used except that $Cu(OAc)_2 \cdot H_2O$ was replaced by $Cu(NO_3)_2 \cdot 3H_2O$ (24 mg, 0.1 mmol) and a 1:1 metal-to-ligand molar ratio was adopted, giving dark blue single crystals in 25% yield (12 mg). Anal. Calcd for {[Cu**L**^{1}(NO$_3$)$_2$](CHCl$_3$)$_{0.5}$}$_n$: C, 30.80; H, 1.76; N, 17.24%. Found: C, 30.23; H, 1.64; N, 17.02%. IR (KBr, cm^{-1}): 3103m, 3018m, 1618vs, 1559m, 1509s, 1499s, 1479vs, 1433s, 1417m, 1384s, 1332m, 1293vs, 1272s, 1240m, 1219m, 1067m, 1016s, 1001s, 837s, 843m, 805m, 757m, 747s, 714s, 609s, 488m.

Synthesis of {[CuL^1(H$_2$O)(SO$_4$)](H$_2$O)$_2$}$_n$, 3. A solution of **L**^{1} (24 mg, 0.1 mmol) in CH_3OH (15 mL) was carefully layered on an aqueous solution (10 mL) of $CuSO_4 \cdot 5H_2O$ (25 mg, 0.1 mmol) in a straight glass tube. After ca. one month, light blue plate single crystals were obtained. Yield: 35 mg (78%). Anal. Calcd for {[Cu**L**^{1}(H$_2$O)(SO$_4$)](H$_2$O)$_2$}$_n$: C, 31.75; H, 3.11; N, 12.34%. Found: C, 32.21; H, 3.13; N, 12.70%. IR (KBr, cm^{-1}): 3427b, 3099m, 3071m, 1611s, 1558m, 1429s, 1330m, 1259w, 1223m, 1149s, 1109vs, 1066m, 1026s, 1004m, 991w, 963m, 829s, 710s, 660m, 618s, 606m, 503w, 484w, 402w.

Synthesis of {[CdL^1(NCS)$_2$](CH$_3$OH)$_{1.5}$}$_n$, 4. A solution of an excess of NH_4SCN (16 mg, 0.2 mmol) in CH_3OH (10 mL) was carefully layered on a $CH_3OH/CHCl_3$ solution (5 mL/10 mL) containing $Cd(ClO_4)_2 \cdot 6H_2O$ (42 mg, 0.1 mmol) and **L**^{1} (24 mg, 0.1 mmol) in a straight glass tube. After ca. one week, block colorless single crystals were obtained. Yield: 39 mg (75%). Anal. Calcd for {[Cd**L**^{1}(NCS)$_2$](CH$_3$OH)$_{1.5}$}$_n$: C, 36.02; H, 2.73; N, 16.26%. Found: C, 36.73; H, 3.23; N, 16.02%. IR (KBr, cm^{-1}): 3481b, 3090m, 3058m, 2925w, 2068vs, 1606vs, 1559m, 1506w, 1427s, 1413m, 1329m, 1282w, 1258w, 1227m, 1215m, 1093w, 1063w, 1015m, 1007m, 825s, 702s, 606s, 531w, 485m.

Synthesis of {[Co(L^1)$_2$(NCS)$_2$](H$_2$O)$_{2.5}$}$_n$, 5. A solution of an excess of NH_4SCN (8 mg, 0.1 mmol) in CH_3OH (10 mL) was carefully layered on a $CH_3OH/CHCl_3$ solution (5 mL/10 mL) containing $Co(ClO_4)_2 \cdot 6H_2O$ (18 mg, 0.05 mmol) and **L**^{1} (24 mg, 0.1 mmol) in a straight glass tube. After ca. one week, block red single crystals were obtained. Yield: 23 mg (65%). Anal. Calcd for {[Co(**L**^{1})$_2$(NCS)$_2$](H$_2$O)$_{2.5}$}$_n$: C, 44.57; H, 3.02; N, 19.99%. Found: C, 44.73; H, 2.93; N, 20.24%. IR (KBr, cm^{-1}): 3424b, 3063m, 2094vs, 2048m, 1647w, 1610m, 1599m, 1557w, 1428s, 1422m, 1400m, 1321m, 1084m, 1064w, 884w, 834m, 824s, 791w, 732w, 702s, 661m, 609s, 498w, 463m.

Synthesis of [Co(L^3)$_2$(NCS)$_2$]$_n$, 6. The same synthetic procedure as for **5** was used except that **L**^{1} was replaced by **L**^{3} (22 mg, 0.1 mmol), giving well-shaped red-violet single crystals in 50% yield (16 mg). Anal. Calcd for [Co(**L**$_3$)$_2$(NCS)$_2$]$_n$: C, 50.08; H, 2.59; N, 22.46%. Found: C, 49.46; H, 2.93; N, 22.54%. IR (KBr, cm^{-1}): 3094w, 2864w, 2057vs, 2012s, 1783w, 1612s, 1551m, 1481s, 1468s, 1435s, 1328m, 1278m, 1199m, 1186m, 1117m, 1085m, 1043s, 966m, 928w, 822m, 806m, 732s, 698s, 640m, 484m, 422m, 406m.

CAUTION! Perchlorate complexes of metal ions in the presence of organic ligands are potentially explosive. Only a small amount of material should be handled with care.

X-ray Data Collection and Structure Determinations. X-ray single-crystal diffraction data for complexes **1**−**6** were collected on a Bruker Smart 1000 CCD diffractometer at 293(2) K with Mo Kα radiation ($\lambda = 0.71073$ Å) by $\phi-\omega$ scan mode. The program SAINT[6] was used for integration of the diffraction profiles. The crystal of **5** is sensitive to air and measured in a sealed capillary. All the structures were solved by direct methods using the SHELXS program of the SHELXTL package and refined by full-matrix least-squares methods with SHELXL (semiempirical absorption corrections were applied using SADABS program).[7] Metal atoms in each complex were located from the E-maps, and other non-hydrogen atoms were located in successive difference Fourier syntheses and refined with anisotropic thermal parameters on F^2. The hydrogen atoms of the ligand were generated theoretically onto the specific atoms and refined isotropically with fixed thermal factors (the hydrogen atoms of the coordianted water molecules in **3** and the solvent molecules were located using difference Fourier method). Further details for structural analysis are summarized in Table 1.

Results and Discussion

Synthesis and General Characterization. Complexes **1**, **2**, and **3** were prepared by the reactions of corresponding Cu^{II} salts with the ligand **L**^{1}, the first two in $CH_3OH/CHCl_3$ and the latter in CH_3OH/H_2O medium (see Scheme 1). The reaction of $Cu(NO_3)_2 \cdot 3H_2O$ with **L**^{1} resulted in two types of crystals with different colors. One was complex **2** with a color of dark blue, as described above. The other unidentified light blue crystals (**2a**), which could not be investigated by X-ray analysis for their poor quality, were obtained later. The composition of **2a** was proved to be definitely different from that of **2** by elemental analyses and IR spectroscopy. The polycrystalline precipitates of complex **3** could be

(6) *SAINT Software Reference Manual*; Bruker AXS: Madison, WI, 1998.
(7) Sheldrick, G. M. *SHELXTL NT Version 5.1. Program for Solution and Refinement of Crystal Structures*; University of Göttingen: Göttingen, Germany, 1997.

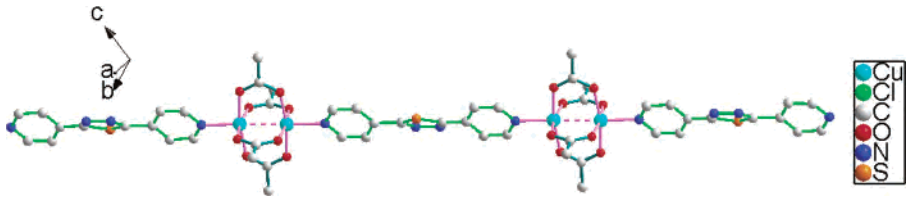

Figure 1. 1D chain structure for **1** (hydrogen atoms and $CHCl_3$ molecules are omitted for clarity).

Scheme 1

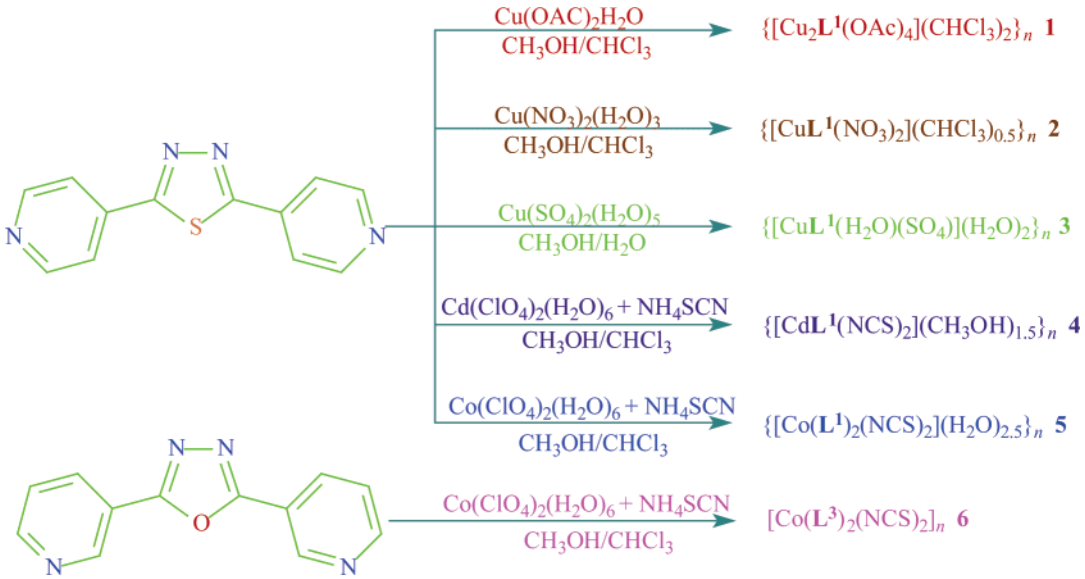

isolated within few minutes using a 1:1 ligand-to-metal molar ratio in a stirring CH_3OH/H_2O solution, which was confirmed by elemental analyses, IR spectroscopy, and XPRD. Complexes **4**, **5**, and **6** were prepared under similar conditions. Similar to **3**, a bulk sample of **4** could be obtained immediately by adding the CH_3OH solution of an excess of NH_4SCN directly to the stirring solution of $CH_3OH/CHCl_3$ containing $Cd(ClO_4)_2 \cdot 6H_2O$ and $\mathbf{L^1}$ in 1:1 molar ratio, which has also been confirmed by elemental analyses, IR spectroscopy, and XPRD. Indeed, the final products for complexes **4**, **5**, and **6** were independent to the quantity of NH_4SCN. The red crystalline samples of **5** are not stable and turn green gradually when exposed to air as stated above. The green substance is amorphous and insoluble in water solution, the composition of which seems to be $\{[Co(\mathbf{L^1})_2(NCS)_2](H_2O)_{1.5}\}_n$ (**5a**) according to the results of the elemental analyses. Exposing the sample of **5a** to water vapor for 72 h to examine if the lost guest water molecule could be reintroduced, however, was negative.

The IR spectra of all six complexes show absorption bonds resulting from the skeletal vibrations of the aromatic rings in the 1400−1600 cm^{-1} range. In the IR spectra of **3**, **4**, and **5**, the broad band centered at ca. 3400 cm^{-1} indicates the O−H stretching of the aqua or CH_3OH solvents. For **1**, the characteristic bands of the acetate anions appear at 1615 $\nu_{as(C-O)}$, 1430 for $\nu_{sym(C-O)}$, and 700 cm^{-1} for $\delta_{(O-C-O)}$. The Δ value ($\nu_{as} - \nu_{sym}$) indicates that the acetate anion coordinates to the Cu^{II} center in bridging mode. For **2**, the characteristic bands of the NO_3^- anions appear at the range 1479−1509 cm^{-1} for ν_a (NO_2), 1293 cm^{-1} for ν_s (NO_2), and 1016 cm^{-1} for ν (NO). The ($\nu_a - \nu_s$) value is in the range 186−216 cm^{-1}, suggesting the bidentate chelated coordination mode of NO_3^- with Cu^{II} center. The IR spectrum for **3** displays the characteristic bands of the SO_4^{2-} anions at 1026−1149 cm^{-1}, 962 cm^{-1}, and 660 cm^{-1}, indicating the monodendate or tridendate coordination feature (C_{3v} symmetry) of SO_4^{2-} groups when coordinated to the Cu^{II} center. The IR spectra show the very strong adsorption bands of the NCS^- groups at 2068, 2094, and 2057 cm^{-1} for complexes **4**, **5**, and **6**, respectively.

X-ray Single-Crystal Structures of Complexes 1−6. $\{[Cu_2L^1(\mu\text{-}OAc)_4](CHCl_3)_2\}_n$**, 1.** The structure of complex **1** consists of a 1-D neutral coordination chain $[Cu_2\mathbf{L^1}(OAc)_4]_n$ and $CHCl_3$ solvent molecules. As shown in Figure 1, the Cu^{II} ion is pentacoordinated to four oxygen atoms of four distinct acetate anions (Cu−O lengths in 1.960(4)−1.978(4) Å region) and one nitrogen atom from the pyridine ring of $\mathbf{L^1}$ (Cu−N = 2.174(4) Å) to form a square-pyramid geometry. The Cu^{II} center deviates from the mean equatorial plane defined by four coordinated oxygen atoms toward the apical nitrogen atom by 0.193 Å. The bond distances and angles (Table 2) are similar to those in its analogues.[4e,g] Four acetate anions bridge two Cu^{II} centers in *syn*−*syn* fashion, to form a $[Cu_2(OAc)_4]$ binuclear building unit, in which the Cu−Cu distance is rather short (2.617(1) Å). This Cu−Cu unit is further linked by the $\mathbf{L^1}$ ligands in a *trans* arrangement and thus generates the 1-D linear chain with the neighboring Cu···Cu separation bridged by $\mathbf{L^1}$ of 15.219 Å. Two pyridyl rings within each $\mathbf{L^1}$ are parallel and related to each other by a crystallographic center of symmetry, which is not observed in the related compounds.[4] The dihedral angle between the thiadiazole and the pyridyl ring is 30.0°.

Table 2. Selected Bond Distances (Å) and Angles (deg) for Complex **1**[a]

Cu(1)−O(1)	1.978(4)	Cu(1)−O(2)	1.960(4)
Cu(1)−O(3)	1.972(4)	Cu(1)−O(4)	1.975(4)
Cu(1)−N(1)	2.174(4)	Cu(1)−Cu(1)#1	2.617(1)
O(2)−Cu(1)−O(3)	90.1(2)	O(2)−Cu(1)−O(4)	90.8(2)
O(3)−Cu(1)−O(4)	168.5(1)	O(2)−Cu(1)−O(1)	168.9(1)
O(3)−Cu(1)−O(1)	88.5(2)	O(4)−Cu(1)−O(1)	88.5(2)
O(2)−Cu(1)−N(1)	93.7(2)	O(3)−Cu(1)−N(1)	92.8(2)
O(4)−Cu(1)−N(1)	98.6(2)	O(1)−Cu(1)−N(1)	97.4(2)

[a] Symmetry operations: #1, $-x+1, -y+1, -z+1$.

Table 3. Selected Bond Distances (Å) and Angles (deg) for Complex **2**[a]

Cu(1)−N(1)	1.983(3)	Cu(1)−O(1)	1.997(3)
Cu(1)−N(4)#1	1.998(3)	Cu(1)−O(4)	2.007(3)
N(1)−Cu(1)−O(1)	90.8(1)	N(1)−Cu(1)−N(4)#1	175.5(1)
O(1)−Cu(1)−N(4)#1	87.0(1)	N(1)−Cu(1)−O(4)	90.3(1)
O(1)−Cu(1)−O(4)	171.3(1)	N(4)#1−Cu(1)−O(4)	91.3(1)

[a] Symmetry operations: #1, $x-1/2, y-1/2, z$.

{[CuL^1(NO$_3$)$_2$](CHCl$_3$)$_{0.5}$}$_n$, 2. In complex **2**, the Cu^{II} ion has a slightly distorted square-planar geometry composed of two oxygen atoms of two NO_3^- anions [Cu−O lengths of 1.997(3) and 2.007(3) Å] and two pyridyl nitrogen atoms from two distinct **L^1** ligands [Cu−N lengths of 1.983(3) and 1.998(3) Å]. Four N−Cu−O bond angles range from 87.0(1)° to 91.31(1)° (Table 3). Weak coordination interactions, such as Cu(1)−O(2) (2.532(4) Å), Cu(1)−O(5) (2.646(1) Å), Cu(1)−N(5) (2.657(7) Å), Cu(1)−N(6) (2.729(4) Å), and Cu(1)−O(4) (2.651(2) Å, the O(4) atom from the NO_3^- also coordinating to another Cu^{II} center), were observed. The deviation of the Cu^{II} center from the mean coordination plane N(1)−N(4)−O(1)−O(4) is 0.110 Å. Different from complexes **1**, **3**, **4**, and **5**, the **L^1** ligands in **2** surrounding the Cu^{II} centers herein are in *cis* arrangement. Within each **L^1** molecule, the dihedral angle between two pyridyl rings is 7.3°.

The bridging feature of **L^1** gives rise to an infinite linear $[-Cu-\mathbf{L^1}-Cu-\mathbf{L^1}-]_n$ chain with the N−Cu−N angle of 175.5(1)°. The intrachain neighboring Cu···Cu distance is 14.784 Å, slightly shorter than that in complex **1** (15.219 Å). Moreover, two neighboring antiparallel chains are ligated together through the weak coordination interactions between the Cu^{II} centers and the NO_3^- anions, as previously noted, to form a 1-D double-chain motif (the shortest interchain Cu···Cu distance is 3.854 Å). Within each double-chain architecture, two nearly parallel pyridyl rings (with a dihedral angle of 7.3°) from the different chains are involved in a $\pi-\pi$ stacking interaction[8] with the center-to-center separation of 3.737 Å (average interplanar separation = 3.683 Å), and so are two strictly parallel thiadiazole rings characterized by the center-to-center separation of 3.532 Å (average interplanar separation = 3.489 Å). Actually, such intermolecular aromatic contacts in this case should be considered as an effective force for the formation of this double-chain motif.[8b] These double-chains extend in two directions (with respect to each other by a 36.6° rotation) and stack alternating along the [001] direction (Figure 2b), leaving space occupied by the disordered $CHCl_3$ molecules. A very similar structure based on 1,2-bis(4-pyridyl)ethylene and $Cu(NO_3)_2\cdot 3H_2O$ has been reported by Carlucci et al.[3e]

Table 4. Selected Bond Distances (Å) and Angles (deg) for Complex **3**[a]

Cu(1)−O(1)	1.978(3)	Cu(1)−O(5)	1.982(3)
Cu(1)−N(1)	2.020(3)	Cu(1)−N(4)#1	2.038(3)
Cu(1)−O(4)#2	2.396(3)		
O(1)−Cu(1)−O(5)	171.9(1)	O(1)−Cu(1)−N(1)	90.4(1)
O(5)−Cu(1)−N(1)	88.4 (1)	O(1)−Cu(1)−N(4)#1	88.7(1)
O(5)−Cu(1)−N(4)#1	92.7(1)	N(1)−Cu(1)−N(4)#1	177.7(1)
O(1)−Cu(1)−O(4)#2	86.1(1)	O(5)−Cu(1)−O(4)#2	85.9(1)
N(1)−Cu(1)−O(4)#2	90.5(1)	N(4)#1−Cu(1)−O(4)#2	91.6(1)

[a] Symmetry operations: #1, $-x+3/2, -y, z+1/2$; #2, $-x+1, y+1/2, -z+1/2$.

{[CuL^1(H$_2$O)(SO$_4$)](H$_2$O)$_2$}$_n$, 3. Complex **3** is a more interesting material, which crystallizes in chiral space group $P2_12_12_1$. It consists of a neutral 3-D porous network with guest water molecules included in the pores. The Cu^{II} ion coordinates to one aqua oxygen atom, two oxygen atoms of two SO_4^- anions, as well as two pyridyl nitrogen atoms from distinct **L^1** ligands (Figure 3a). The bond distance of Cu(1)−O(4) (2.396(3) Å) is longer compared with those of the remaining Cu−O (1.978(3) and 1.982(3) Å) or Cu−N (2.020(3) and 2.038(3) Å) lengths. Moreover, each Cu^{II} center also presents one long contact (Cu(1)−O(3) = 2.625(1) Å) with one oxygen atom from the third SO_4^- anion. Taking into account this weak interaction, the coordination geometry of the Cu^{II} center can be described as a distorted octahedron with Jahn−Teller distortion.

As shown in Figure 3b, each SO_4^- anion bridges three Cu^{II} ions in a μ_3 coordination mode to form a 2-D (6,3) sheet in crystallographic *ab* plane (regarding the sulfur and copper atoms as the connecting nodes). The basic motif of the 2-D layer is the $[Cu_3(\mu_3\text{-}SO_4)_3]$ ring, in which three anion-bridged Cu···Cu distances are 5.509, 5.903, and 6.088 Å, respectively. The Cu−O bond vector of the coordinated aqua is on the coordination sheet plane. These sheets are further connected by **L^1** in a *trans* arrangement along the [001] direction to form a 3-D open framework. The topology of this network has the Schäfli symbol $(6^3).(6^9.8)$. The neighboring Cu···Cu distance connected by **L^1** is 14.704 Å. Within each **L^1**, two pyridyl rings bent to the same direction with a dihedral angle of 6.7°. Two types of centrosymmetrical openings are created in this network along the [100] direction (Figure 3c). The larger channels with the dimensions of ca. 14 Å × 6 Å are occupied by two uncoordinated water molecules, which represent ca. 19.9% of the total volume of the unit cell.[9] The structure of **3** is isomorphic to that of $\{[Cu\mathbf{L^2}(H_2O)(SO_4)](H_2O)_2\}_n$, indicating such 3-D structure is thermodynamically stable.[4h]

(8) (a) Janiak, C. *J. Chem. Soc., Dalton Trans.* **2000**, 3885. (b) Khlobystov, A. N.; Blake, A. J.; Champness, N. R.; Lemenovskii, D. A.; Majouga, A. G.; Zyk, N. V.; Schröder, M. *Coord. Chem. Rev.* **2001**, *222*, 155 and references therein.

(9) Analysis of the voids was performed with the PLATON program: Spek, A. L. *Platon, A Multipurpose Crystallographic Tool*; Utrecht University: Utrecht: The Netherlands, 1999.

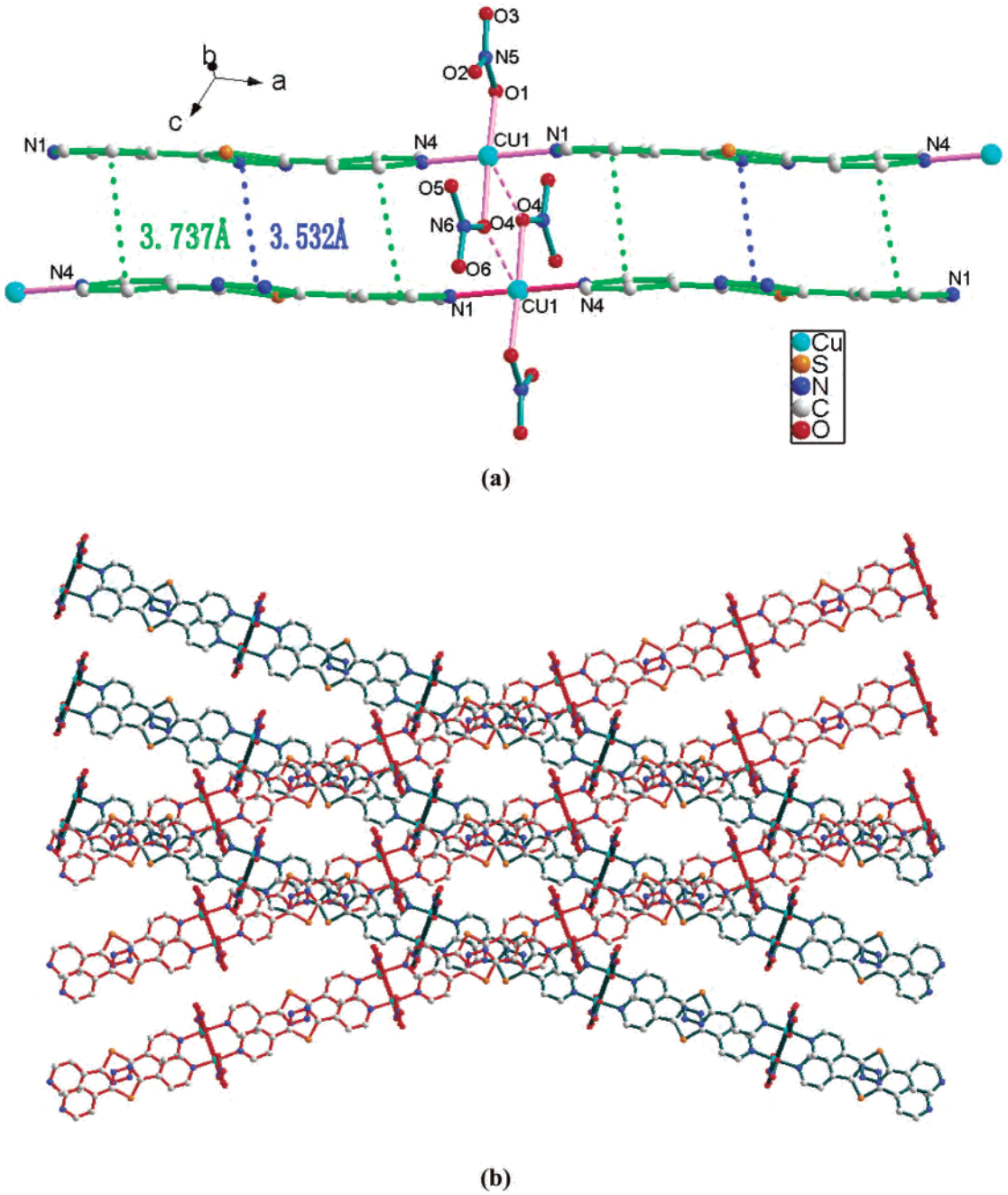

Figure 2. (a) View of the double-chain structure for **2** (hydrogen atoms and $CHCl_3$ molecules are omitted for clarity); (b) stacking diagram along [001] direction (different colors of the bonds are used to shown the double-chains extending in two direction).

{[CdL¹(NCS)₂](CH₃OH)₁.₅}*n*, 4. The structure of **4** also has a 3-D coordination framework, in which the Cd^{II} ion is six-coordinated to two nitrogen atoms and two sulfur atoms of four distinct NCS^- groups, as well as two pyridyl nitrogen atoms from two $\mathbf{L^1}$ ligands. The metal center has an elongated octahedral coordination geometry with two longer Cd−S bonds ($Cd-S_{NCS}$ = 2.722(2) Å) in the axial positions, and four shorter Cd−N bonds ($Cd-N_{py}$ = 2.368(3) Å, $Cd-N_{NCS}$ = 2.309(3) Å) in the equatorial plane. The *cis* N−Cd−N and N−Cd−S bond angles range from 87.76(9)° to 92.24(9)° (Table 5). Both $\mathbf{L^1}$ and NCS^- ligands herein are coordinated in a *trans* fashion. The geometry of the NCS^- group is linear with the N−C−S angle of 179.59(2)°. The two pyridyl rings within each $\mathbf{L^1}$ deviate by 19.4° from coplanarity.

Table 5. Selected Bond Distances (Å) and Angles (deg) for Complex **4**[a]

Cd(1)−N(3)#1	2.309(3)	Cd(1)−N(1)	2.368(3)
Cd(1)−S(2)	2.722(2)		
N(3)#1−Cd(1)−N(1)#3	91.5(1)	N(3)#2−Cd(1)−N(1)#3	88.5(1)
N(3)#1−Cd(1)−S(2)#3	89.81(9)	N(3)#2−Cd(1)−S(2)#3	90.19(9)
N(1)#3−Cd(1)−S(2)#3	92.24(9)	N(1)−Cd(1)−S(2)#3	87.76(9)
C(7)−N(3)−Cd(1)#4	165.2(3)	C(7)−S(2)−Cd(1)	98.8(1)
N(3)−C(7)−S(2)	179.6(4)		

[a] Symmetry operations: #1, $x, -y+2, z-1/2$; #2, $-x+1/2, y-1/2, -z+1/2$; #3, $-x+1/2, -y+3/2, -z$; #4, $-x+1/2, y+1/2, -z+1/2$.

The overall array of **4** is somewhat similar to that of **3**; both of them are constructed by linking the 2-D metal−anion layers through $\mathbf{L^1}$−metal−$\mathbf{L^1}$−metal chains. Different from **3**, however, herein each bridging NCS^- group links two

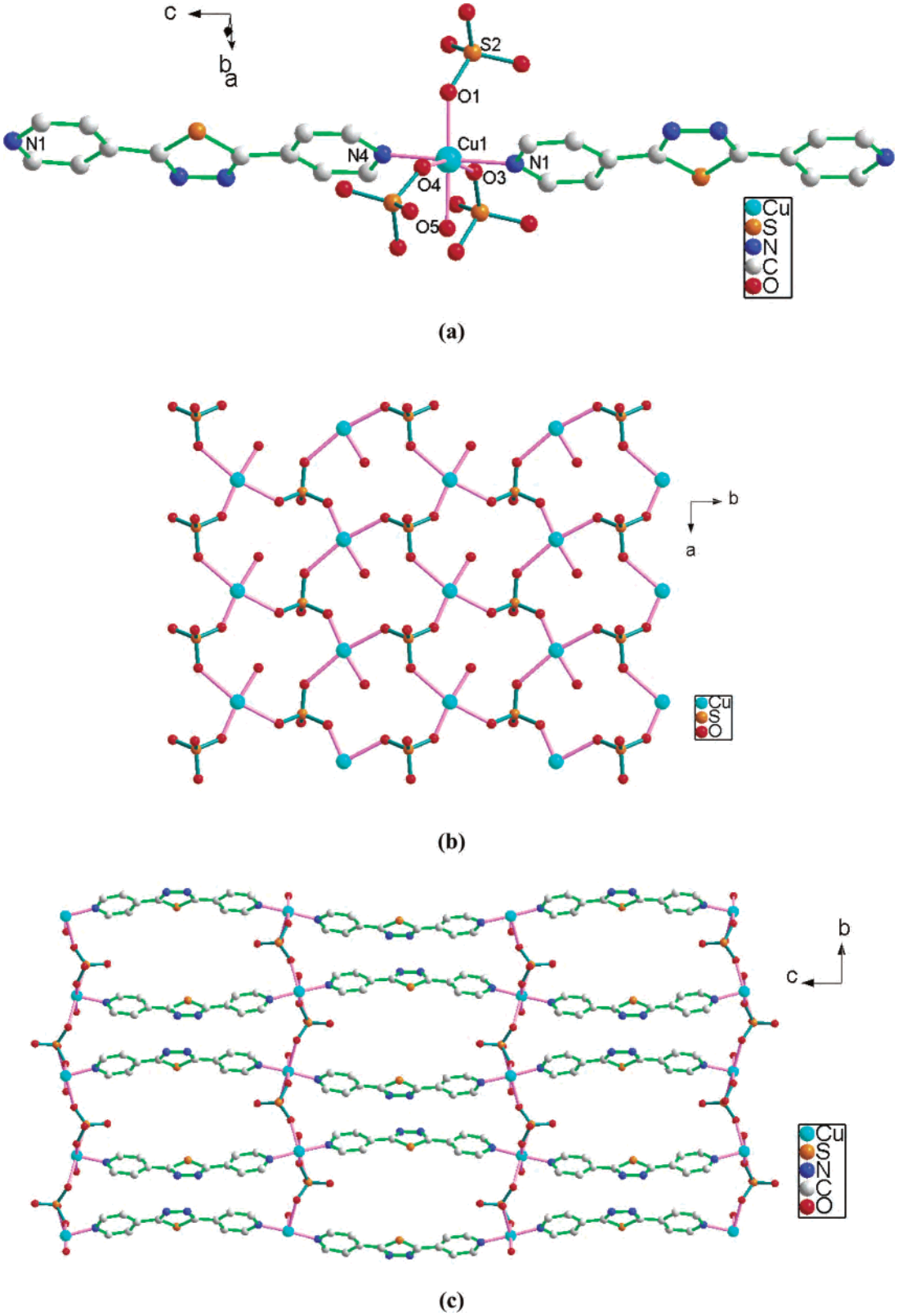

Figure 3. (a) View of the metal coordination environment in **3** (hydrogen atoms and water molecules are omitted for clarity); (b) 2-D (6,3) sheet consisting of μ_3 bridging sulfate anions and metal ions; (c) the chiral 3-D structure with channels along [100] direction.

adjacent Cd^{II} centers to form a 2-D sheet with common (4,4) topology along the *bc* plane consisting of 16-membered $[Cd_4(\mu\text{-NCS-}N,S)_4]$ macrocycles (Figure 4b). The Cd^{II} centers in each layer are disposed at the nodes of a rhombic grid with the NSC-bridging Cd···Cd distance of 6.207 Å. The angles of Cd(1)−S(2)−C(7) and Cd(1)−N(3)−C(7) are 98.8-(1)° and 165.2(3)°, respectively. Furthermore, each $\mathbf{L^1}$ links two Cd atoms from the neighboring layers with the $\mathbf{L^1}$-bridging Cd···Cd distance of 15.220 Å. The angular geometry of $\mathbf{L^1}$ (the angle between the central thiadiazole ring

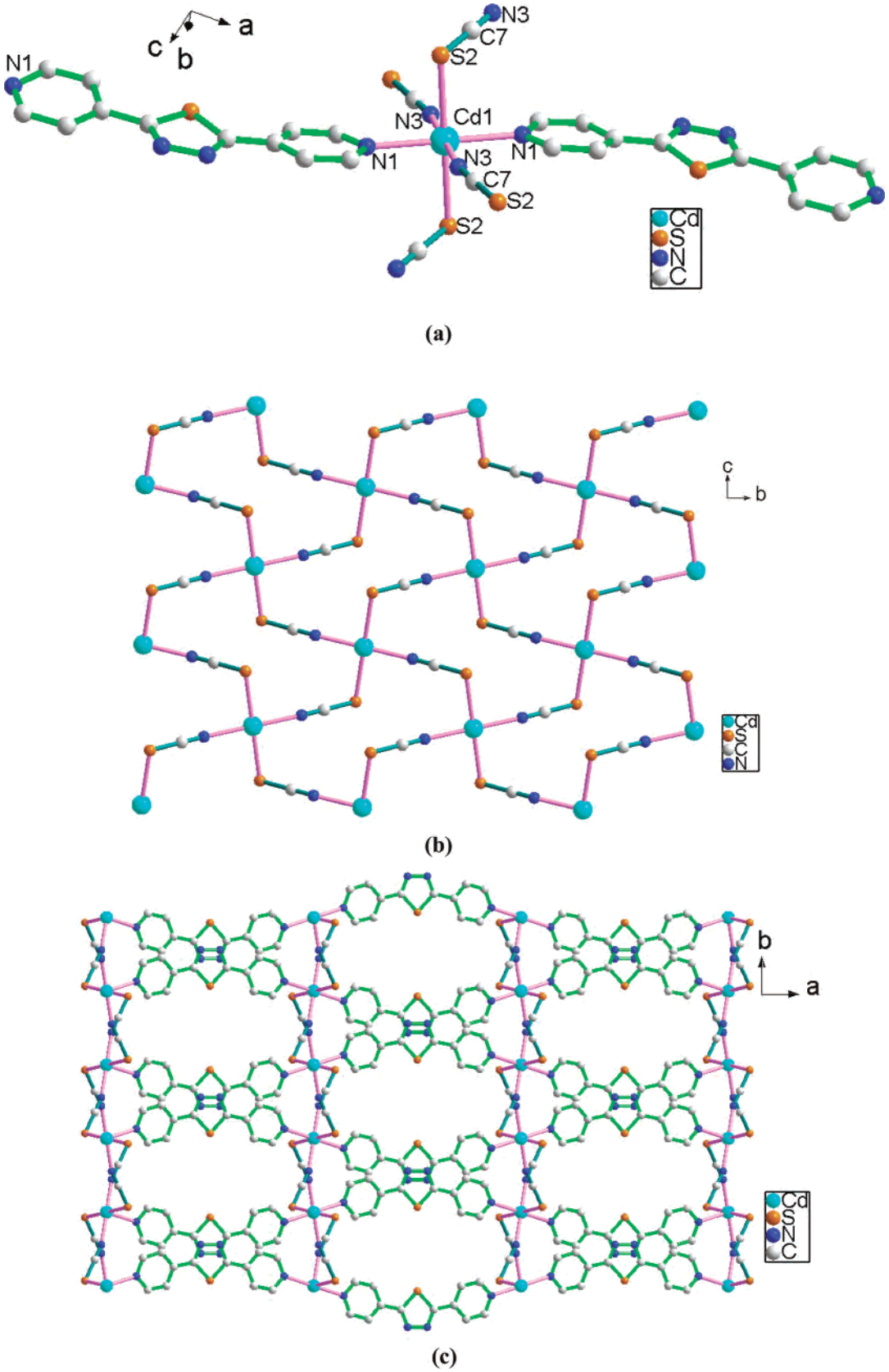

Figure 4. (a) View of the metal coordination environment in **4** (hydrogen atoms and CH_3OH molecules are omitted for clarity); (b) view of the 2-D metal−anion sheet in the *bc* plane; (c) the 3-D open structure with channels running down the *c* axis.

and two *N*-donors of the 4-pyridyl ring is 155.3°), together with the *trans* arrangement mode of $\mathbf{L^1}$ around the Cd^{II} center, results in the $\mathbf{L^1}$−Cd−$\mathbf{L^1}$−Cd chains with "sinusoidal" geometry. Along these chains, the parallel 2-D $[Cd_4(\mu\text{-NCS-}N,S)_4]_n$ layers are bound together to generate a 3-D open network containing elliptical channels parallel to the *c*

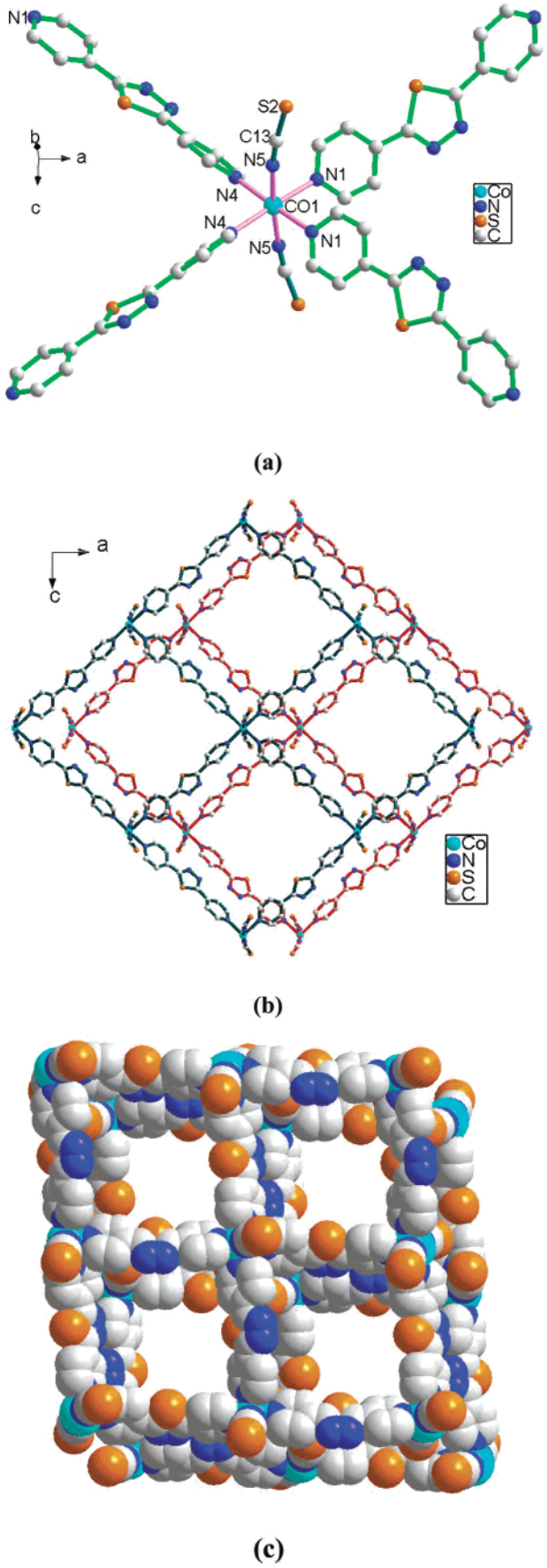

Figure 5. (a) View of the metal coordination environment in **5** (hydrogen atoms and water molecules are omitted for clarity); (b) view of the stacking of the sheets along *b* axis (different colors of the bonds are used to shown the staggered sheets); (c) the open channel running down the *b* axis are evidenced.

Table 6. Selected Bond Distances (Å) and Angles (deg) for Complex **5**[a]

Co(1)−N(5)	2.080(9)	Co(1)−N(4)#2	2.175(3)
Co(1)−N(1)	2.188(3)		
N(5)−Co(1)−N(5)#1	175.0(19)	N(5)−Co(1)−N(4)#2	90.3(11)
N(4)#2−Co(1)−N(4)#3	89.9(2)	N(5)−Co(1)−N(1)#1	87.3(11)
N(5)#1−Co(1)−N(1)#1	89.2(10)	N(4)#2−Co(1)−N(1)#1	177.5(1)
N(4)#3−Co(1)−N(1)#1	90.9(1)	N(5)−Co(1)−N(1)	89.2(10)
N(1)#1−Co(1)−N(1)	88.3(2)	N(5)#1−Co(1)−N(4)#2	93.2(10)
C(13)−N(5)−Co(1)	167(3)	N(5)−C(13)−S(2)	174(3)

[a] Symmetry operations: #1, $x, -y + {}^1/_2, -z + {}^1/_2$; #2, $x - {}^1/_2, y, -z$; #3, $x - {}^1/_2, -y + {}^1/_2, z + {}^1/_2$.

axis with the dimensions of ca. 13 Å × 5 Å. These channels are not empty, and are filled with the disordered CH_3OH molecules, which account for 25.4% of the total crystal volume. A similar host framework consisting of $[Cd\mathbf{L^2}(NCS)_2]_n$ was reported recently, the voids of which are occupied by the CH_3CN guest molecules.[4b]

$\{[Co(L^1)_2(NCS)_2](H_2O)_{2.5}\}_n$, 5. The coordination environment of the Co^{II} ion in **5** is shown in Figure 5a. Each metal center is six-coordinated to two NCS^- groups and four $\mathbf{L^1}$ ligands. The Co−N distance involving the NCS^- group ($Co-N_{NCS}$ = 2.080(9) Å) is shorter than the $Co-N_{py}$ lengths (2.175(3) and 2.188(3) Å). It is clear that each Co^{II} center lies in a slightly distorted octahedral environment with the *cis* N−Co−N angles being in the range 87.3(11)°−93.2(10)°. The *trans* N−Co−N bond angles for NCS^- and $\mathbf{L^1}$ ligands are 175.0(19)° and 177.5(1)°. The two pyridyl rings within each $\mathbf{L^1}$ deviate by 23.6° from coplanarity. The NCS^- ligands are coordinated axially in a terminal mode with the angles of 167(3)° for Co(1)−N(5)−C(13) and 174(3)° for N(5)−C(13)−S(2). Selected bond distances and angles for **5** are listed in Table 6.

Figure 5b shows the lamellar network of **5**, in which the adjacent Co^{II} centers are linked by the bridging $\mathbf{L^1}$ in two different directions to form large and nearly square repeating grids (the ligand-bridging Co···Co distance is 15.022 Å and the internal angles of each square are 84.66° and 95.34°), forming a 2-D (4,4) sheet. These sheets are stacked along the *b* axis with an ABAB sequence, offset by approximately $0.25(a + c)$ along the *ac* plane so that large channels are created with a square cross section (ca. 9 Å × 9 Å), as illustrated in Figure 5b. The stacking separation between two adjacent sheets is ca. 6.4 Å, and the shortest intersheet Co···Co distance is 8.505 Å. The disordered water molecules (2.5 per formula unit) are incorporated in the channels and the interlayer regions. An analysis of the voids of **5** shows ca. 32.0% of the space empty even if calculating the water molecules, and after the removal of these solvents, the empty space adds up to 47.0%.

We have used $\mathbf{L^2}$ to react with $Co(NCS)_2$ in a $CH_3CN/CHCl_3$ medium, affording a mononuclear complex $[Co(\mathbf{L^2})(NSC)_2(H_2O)_2]$, whose extended structure contrasts greatly with that of complex **5**.[4d] At first we considered that this discrepancy may result from the different solvents, as described in the literature.[10] However, our further experiments showed the crystals of **5** could also be obtained by the reaction of $\mathbf{L^1}$ with $Co(SCN)_2$ in various media, such as

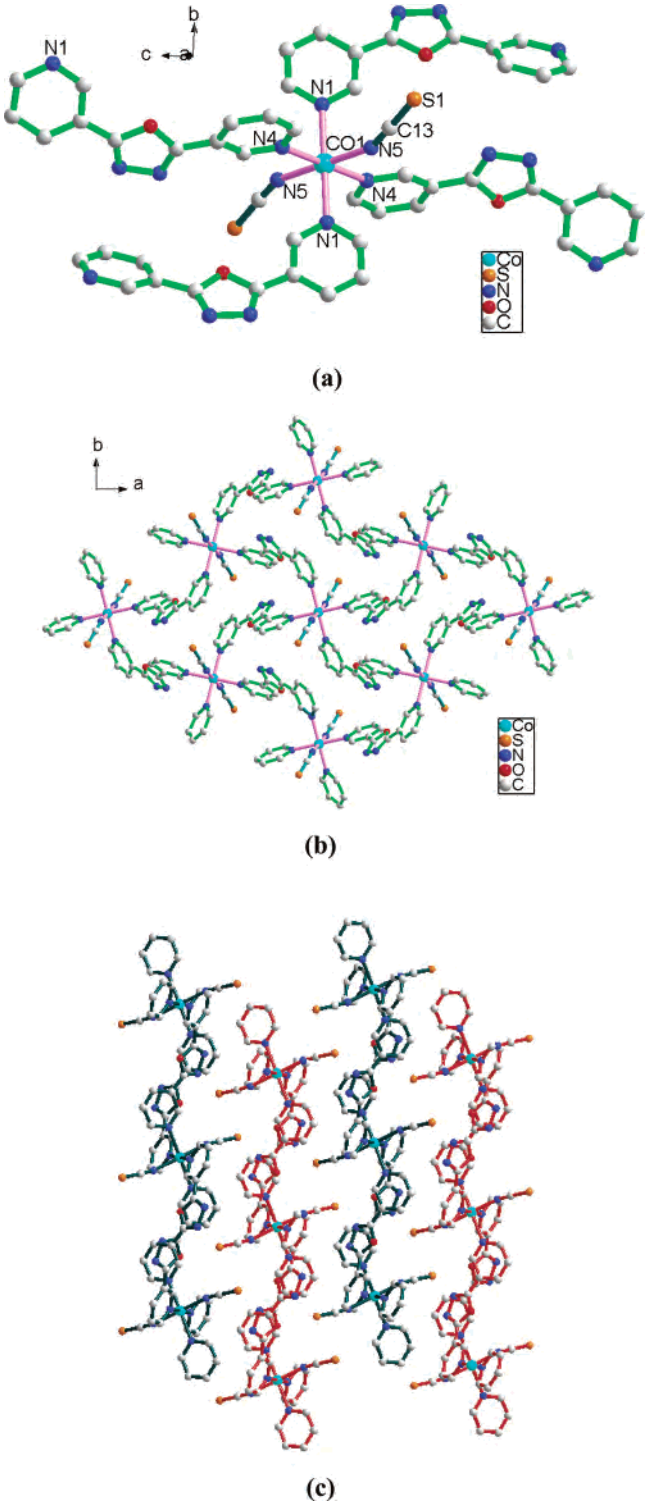

Figure 6. (a) View of the metal coordination environment in **6** (hydrogen atoms are omitted for clarity); (b) 2-D sheet which is the projection view along *a* direction; (c) view of the stacking of the adjacent sheets along *b* axis (different colors of the bonds are used to shown the staggered sheets).

$CH_3CN/CHCl_3$, $EtOH/CHCl_3$, and CH_3OH/H_2O, and this indicates that the formation of complex **5** is independent to the choice of the solvents.

(10) (a) Lu, J.; Paliwara, T.; Lim, S. C.; Yu, C.; Niu, T.; Jacobson, A. J. *Inorg. Chem.* **1997**, *36*, 923. (b) Withersby, M. A.; Blake, A. J.; Champness, N. R.; Cooke, P. A.; Hubberstey, P.; Li, W.-S.; Schröder, M. *Inorg. Chem.* **1999**, *38*, 2259.

Table 7. Selected Bond Distances (Å) and Angles (deg) for Complex **6**[a]

Co(1)−N(5)	2.077(3)	Co(1)−N(1)	2.178(3)
Co(1)−N(4)#2	2.247(3)		
N(5)#1−Co(1)−N(1)	88.3(1)	N(5)−Co(1)−N(1)	91.7(1)
N(1)#1−Co(1)−N(4)#2	88.3(1)	N(1)−Co(1)−N(4)#2	91.7(1)
C(13)−N(5)−Co(1)	157.2(3)	N(5)−C(13)−S(1)	177.4(3)

[a] Symmetry operations: #1, $-x, -y+1, -z+1$; #2, $-x+1, y+{}^1/_2, -z+{}^3/_2$.

$[Co(L^3)_2(NCS)_2]_n$, 6. The coordination environment of Co^{II} ion in complex **6** is similar to that in **5** (Figure 6a). Each Co^{II} center, being located at the inversion center, is in a compressed octahedral environment composed of two nitrogen atoms of two NCS^- groups in the axial positions and four pyridyl nitrogen atoms from four $\mathbf{L^3}$ molecules in the equatorial plane. The bond distance of the $Co-N_{NCS}$ (2.077(3) Å) is shorter than that of $Co-N_{py}$ [Co−N(1) = 2.178(3) Å, Co−N(4) = 2.247(3) Å], and the *cis* N−Co−N bond angles fall in the range 88.3(1)−91.8(1)°. The NSC^- groups act as terminal ligands in a bent mode with the Co(1)−N(5)−C(13) bond angle of 157.2(3)°. Selected bond distances and angles are listed in Table 7. In contrast to **5**, where they are in a *cis* coordination fashion, herein two terminal NCS^- groups are coordinated axially in a *trans* fashion. Two pyridyl rings within each $\mathbf{L^3}$ ligand deviate by 38.7° from coplanarity.

The $\mathbf{L^3}$ ligand adopts a *trans* conformation, and each bridges two Co^{II} centers to give a 2-D (4,4) sheet, featuring "double-edged axe-shaped" $[Co_4(\mathbf{L^3})_4]$ macrocycles as subunits. The Co^{II} atoms are disposed at the nodes of a rhombic grid in the undulating $[Co(\mathbf{L^3})_2(SCN)_2]_n$ layer with the ligand-bridging Co···Co distance of 11.559 Å (Figure 6b). These layers are stacked in an offset fashion with an ABAB sequence, resulting in interdigitation of the coordination NCS^- groups in the cavities of the adjacent network (Figure 6c). Different from complex **5**, such closely packed layered structure in **6** leaves no free space to accommodate guest molecules. The shortest intersheet Co···Co distance is 8.120 Å.

Comparing the structures of three thiocyanate-containing complexes **4**−**6**, we find the NCS^- groups take monodentate coordination mode and serve as terminal groups in **5** and **6**; however, both Cd−NCS and Cd−SCN coordination fashions are preferable, and the NCS^- group serves as bridging ligand in **4**. This maybe results from the different natures of the Co^{II} and Cd^{II} ions.

Exclusion and Inclusion of Guest Molecules: **TGA and XRPD Studies.** Coordination polymers possessing porous channels are especially of great interest due to their unique properties. As described above, both complexes **3** and **4** have the appealing 3-D frameworks exhibiting open channels filled with guest molecules. The free void, if omitting the guest molecules, is 19.9% of the cell volume for **3** and 25.4% for **4**. The question arises as to whether the framework or the structural regularity will be maintained after the removal of the guest molecules, which is essentially important for generating the new microporous materials. To verify this, we adopt TGA and XRPD techniques to investigate the

framework stability and removal−reintroduction the guest molecules of complexes **3** and **4**.

For **3**, the TGA reveals there is a weight loss (found: 7.82%) from ca. 80 to 130 °C, corresponding to the loss of the free water molecules (calcd: 7.94%). The polycrystalline sample is stable up to 340 °C above which the decomposition starts. According to the TGA results, the freshly ground sample of **3** is evacuated at 160 °C for 6 h. It consequently experiences weight losses being consistent with the removal of two included water molecules per formula unit, which is also confirmed by elemental analyses. The similarity between the XPRD pattern recorded at this point and that of the original starting sample suggests the dried solid $\{[Cu\mathbf{L^1}\text{-}(H_2O)(SO_4)]\}_n$ retains the initial crystal structure of **3**. The slight shift and splitting of some peaks may be attributed to the subtle change of the relative positions of some atoms in the crystal lattice.[4b] The guest water species, however, can be reintroduced into the porous sample of **3** by exposure to water vapor for 10 h, which is confirmed by XRPD (Figure 7), the weight gain of the sample, and elemental analyses. During this repetition, a vivid color change of this material occurs, from light blue for the original sample, to bottle green for the desolvated sample, and to light blue again for the final product. The color change, from another point of view, also proves the feature of reversible exclusion and inclusion of the guest molecules of **3**.

For **4**, TGA reveals the CH_3OH molecules are eliminated from the network on raising the temperature from room temperature to ca. 90 °C (a weight loss of 7.20% is a little smaller than the calculated value, 9.23%, probably resulting from the sensitivity to temperature and humidity or a very slow liberation of the guest molecules from **4** at room temperature), corresponding to the loss of CH_3OH molecules. The decomposition of the framework begins only above ca. 280 °C. Upon evacuation of the freshly ground sample of **4** at 160 °C for 6 h, it experiences weight losses that are consistent with the removal of 1.5 included CH_3OH molecules per formula unit, which is also confirmed by elemental analyses. To our surprise, though the dried solid $[Cd\mathbf{L^1}\text{-}(NCS)_2]_n$ still gives a sharp XPRD pattern, this pattern is not coincident with that of the original sample. Thus, we conclude that the structure of the dried empty solid is changed, but its structural regularity is maintained after the removal of the guest molecules. Notably, the desolvated sample of **4** can regain CH_3OH molecules and interestingly revert to the original structure by exposure to CH_3OH vapor for 2 h, which is also confirmed by XRPD (Figure 8), the weight gain of the sample, and elemental analyses.

The above results demonstrate two potentially different microporous materials: **3** represents one type of complex, which has rigid vacant channels after the removal of the guest molecules, and the structure of the empty sample coincides with that of the original material; **4** represents another type of framework which has the property that removal of guest molecules makes a structural change in the network, however, it can revert to the original structure by reintroducing the guest molecules. The desolvated solids of **3** and **4** may be applied as adsorbents of some small guest molecules.

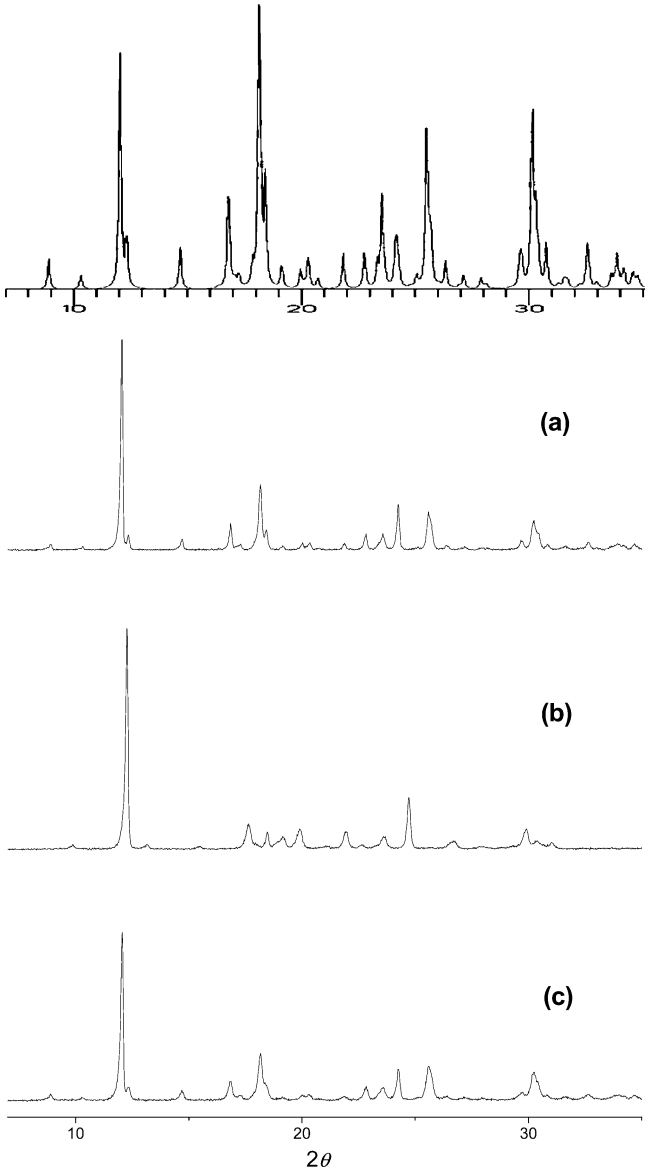

Figure 7. XPRD patters for **3**: (top) calculated; (a) taken at room temperature; (b) after removal of the guest water molecules; (c) after reintroduction of the guest water molecules.

Magnetic Properties. For complex **1**, the susceptibility curve (Figure 9a) shows a round maximum at 270−280 K, indicating a very strong antiferromagnetic coupling. At very low temperature, there is a clear increase of the χ_M values, indicating a small percentage of monomeric Cu^{II} impurities. The temperature dependent on the $\chi_M T$ (per two Cu^{II} ions) is also indicative of this strong antiferromagnetic coupling: it starts at 0.43 $cm^3\ mol^{-1}$ K (much more lower than the value of two noncoupling Cu^{II} ions, 0.80 $cm^3\ mol^{-1}$ K) and tends to zero from 50 to 2 K (Figure 9a). We have analyzed its magnetic data through a simple Bleaney−Bowers expression, derived from the isotropic spin Hamiltonian $H = -JS_1S_2$, with local spins $S = {}^1/_2$,[11] adding a ρ factor as monomeric paramagnetic impurities. The best-fit parameters are $J = -311.0 \pm 1\ cm^{-1}$, $g = 2.10 \pm 0.01$, $\rho = 0.01$, and an agreement factor $R = 6.5 \times 10^{-6}$.

(11) Kahn, O. *Molecular Magnetism*; VCH: Heidelberg, 1993.

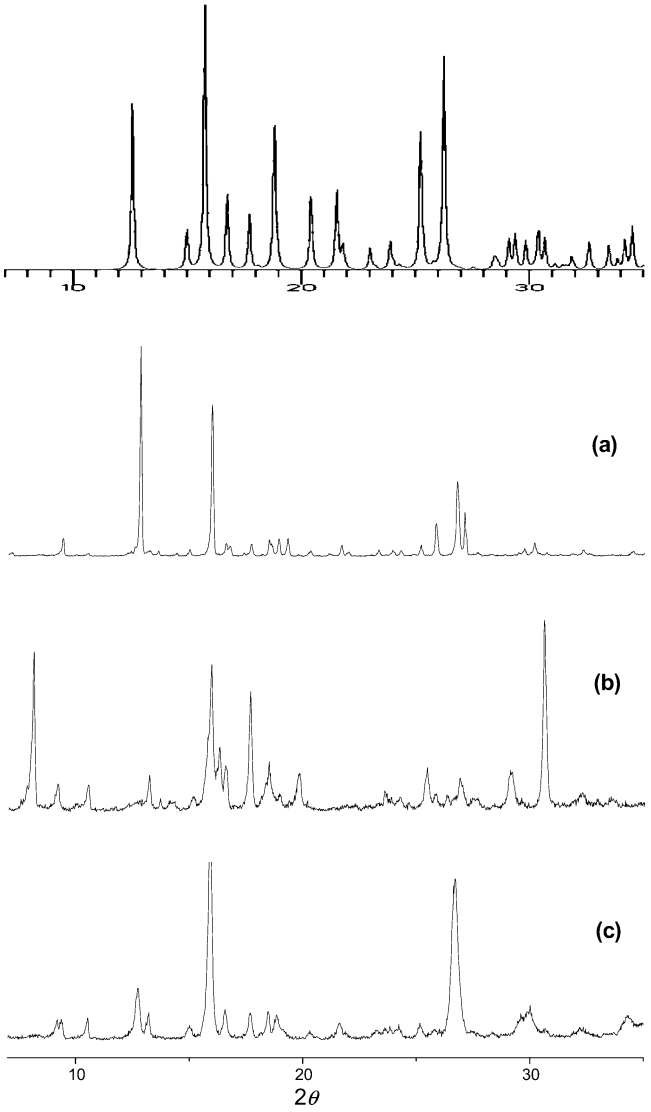

Figure 8. XPRD patters for **4**: (top) calculated; (a) taken at room temperature; (b) after removal of the guest CH_3OH molecules; (c) after reintroduction of the guest CH_3OH molecules.

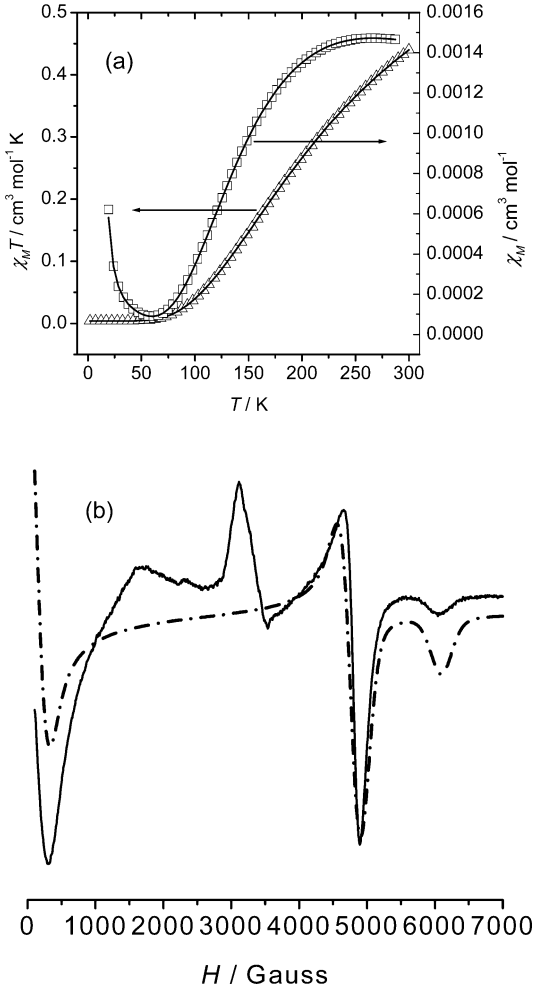

Figure 9. (a) Plot of the χ_M and $\chi_M T$ vs T for **1**. Straight lines correspond to the best fit according to the parameters given in the text. (b) Electron paramagnetic resonance of **1** at room temperature, showing the typical pattern for an $S = 1$ excited state. The dotted line is the simulation made with the D and g values given in the text.

The large antiferromagnetic coupling observed in this compound is in agreement with those observed in the large family of tetra-μ-carboxylato-O,O'-dicopper(II) complexes, where the most common value observed is about -300 cm^{-1}.[12] The presence of the small percentage of impurities avoids the possible calculation of the coupling between the long organic ligands which should give a very small (almost nil) coupling.

The very strong antiferromagnetic coupling between tetra-μ-carboxylato-O,O'-dicopper(II) unit can also be manifested by the ESR spectra at different temperatures. At room temperature, the pattern of the $S = 1$ excited state (populated at this temperature) is very indicative and can be related to the strength of the coupling, as indicated by several publications.[13] For J values close to -300 cm^{-1}, the D parameters is close to 0.5 cm^{-1} and g_z can be very high, such as 2.5. For complex **1**, the ESR spectrum at room temperature together with its simulation is shown in Figure 9b. The best simulation gives the following values: $D = 0.47$ cm^{-1}; $E = 0$ cm^{-1}; $g_x = g_y = 2.12$ and $g_z = 2.55$ (isotropic bandwidth = 300 G). The band which appears in the region of 3000 G in the experimental spectrum is due to the $|0, -1>$ (ground-excited state) and from the impurities of monomeric Cu^{II} ions. Effectively, by lowering the temperature to 4 K, only this band centered at 3000 G remains, with all other bands disappearing, which indicates the depopulation of the excited $S = 1$ state, due to the strong coupling, as indicated above.

The magnetic properties of complexes **2** and **3** are very similar, almost identical. As a representative example, $\chi_M T$ (χ_M is the molar magnetic susceptibility for one Cu^{II} ion) and reduced magnetization, $M/N\beta$, (inset) plots for complex **2** are shown in Figure 10. The value of $\chi_M T$ at 300 K is 0.41 cm^{3}mol^{-1}K, which is as expected for magnetically quasi-isolated spin doublets ($g > 2.00$). $\chi_M T$ values are almost constant to 50 K and below 50 K decrease quickly to 0.20 cm^3 mol^{-1} K at 2 K. The global feature is

(12) Dalai, S.; Mukherjee, P. S.; Zangrando, E.; Lloret, F.; Chaudhuri, N. R. *J. Chem. Soc., Dalton Trans.* **2002**, 822 and references therein.
(13) Muto, Y.; Nakashima, M.; Tokii, T.; Suzuki, I.; Ohba, S.; Steward, O. W.; Kato, M. *Bull. Chem. Soc. Jpn.* **2002**, *75*, 511 and references therein.

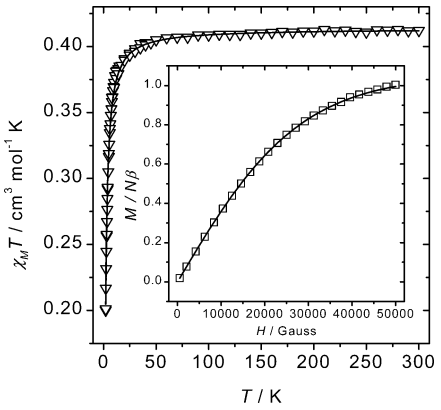

Figure 10. Plot of the temperature dependence of $\chi_M T$ for **2**. The solid line indicates the best fit representation according to the parameters given in the text. Inset: plot of the reduced magnetization ($M/N\beta$) vs H for **2**. The magnetic data for **3** are practically identical.

characteristic of very weak antiferromagnetic interactions. The reduced molar magnetization plot versus H of complex **2** at 2 K (Figure 10 inset) clearly corroborates that the antiferromagnetic coupling is very small. The $M/N\beta$ value at 5 T is close to 1 Nβ, and the curve follows the Brillouin law, assuming $g = 2.11$.

Complexes **2** and **3** are magnetically one-dimensional systems with very long Cu···Cu distances (14.784 Å for **2** and 14.704 Å for **3**), due to the organic bridge that links the Cu^{II} centers. This feature gives uniform $S = {}^1/_2$ systems with J coupling parameter for the Cu−bridge−Cu pathway. The fit of the magnetic data has been carried out with the Clumag program,[14] modeling the input with 12 cycled Cu^{II} atoms, which is the typical number taken in these cases of Cu^{II}, as it approaches an infinite number. The best-fit parameters obtained with this computing model are $J = -1.6 \pm 0.1$ cm^{-1}, $g = 2.10 \pm 0.01$, and $R = 1.2 \times 10^{-5}$ for **2** and $J = -1.7 \pm 0.1$ cm^{-1}, $g = 2.12 \pm 0.01$, and $R = 1.6 \times 10^{-5}$ for **3**. The coincidence between the two J values agrees with the existence of the same bridge in complexes **2** and **3**. The only "noninnocent" difference between **2** and **3** is the terminal ligand: nitrate for **2**, which links two chains through the O4 atom of the nitrate group, but with Cu1−O4 distances at 2.651(2) Å in apical−equatorial positions, and sulfate for **3,** which gives a three-dimensional structure with Cu1−O3 and Cu1−O4 distances at 2.625(1) and 2.396(3) Å, respectively, in axial−equatorial position (see structural details). The small J values can be interpreted, thus, as a consequence of the almost nil overlap between the Cu^{II} ions through the long ligands and through the packing between the one-dimensional entities in the corresponding nets. For the two Cu^{II} complexes **2** and **3**, the Cu···Cu distances are almost the same, and the torsion angle between the two pyridyl rings is small (7.3° for **2** and 6.7° for **3**). The Cu^{II} ion is placed almost perpendicular to the π system, avoiding any possible magnetic pathway. Thus, the magnetic coupling should be very small, as experimentally found.

(14) CLUMAG Program: Gatteschi, D.; Pardi, L. *Gazz. Chim. Ital*. **1993**, *123*, 231. This program uses a full-diagonalization procedure, employing the irreducible tensor operator formalism (ITO).

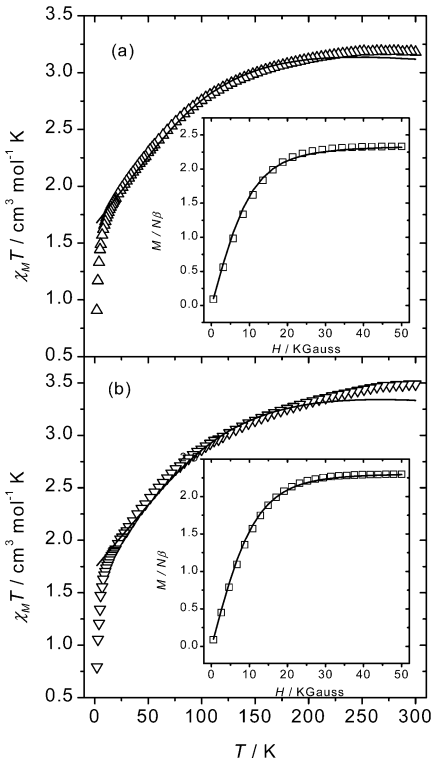

Figure 11. Plots of the temperature dependence of $\chi_M T$ for **5** (a) and **6** (b). The solid lines indicate the best fit representation as mononuclear complexes according to the parameters given in the text. Inset: plot of the reduced magnetization ($M/N\beta$) vs H at 2 K for **5** (a) and **6** (b). The solid line indicates the best fit representation according to the parameters given in the text.

The magnetic properties of complexes **5** and **6** in the form of $\chi_M T$ versus T plots (χ_M is the molar magnetic susceptibility for one Co^{II} ion) and $M/N\beta$ vs H at 2 K (inset) are shown in Figure 11a,b, respectively. $\chi_M T$ values at 300 K are 3.18 cm^3 mol^{-1} K for **5** and 3.48 cm^3 mol^{-1} K for **6**, which are larger than that expected for the spin-only case ($\chi_M T = 1.87$ cm^3 mol^{-1} K, $S = {}^3/_2$), indicating that an important orbital contribution is involved. The $\chi_M T$ values continuously decrease from room temperature to 0.91 cm^3 mol^{-1} K at 2 K for **5** and to 0.79 cm^3 mol^{-1} K for **6**. The reduced molar magnetization ($M/N\beta$) per Co^{II} attends to 2.3 $N\beta$ for **5** and **6**.

The Co···Co distance in complex **5** is 15.022 Å, and the torsion angle between the two pyridyl rings is 23.6°, which avoids any delocalized π-pathway between the Co^{II} ions. In complex **6**, the ligand is different concerning the position of the two *N*-donor atoms, the Co···Co distance is 11.559 Å, but the torsion angle between the pyridyl rings is 38.7°. Thus, even if the Co···Co distance is lower than that in **5**, the torsion angle is greater, avoiding also the possible $\pi-\pi$ delocalized pathway. As a consequence of these structural features, the possible magnetic pathways in **5** and **6** are almost nonexistent, and thus, the magnetic coupling must be almost nil.

A quantitative interpretation of the magnetic data is not straightforward because of the orbital degeneracy of octahedral Co^{II}. As indicated by Antolini et al.,[15] in the noncoupled Co^{II} complexes, the small temperature dependence of $\chi_M T$ down to ca. 100 K rules out any possibility of

relevant antiferromagnetic interaction which might in principle also reduce the room-temperature effective magnetic moment. The observed decrease of $\chi_M T$ at lower temperature can be attributed to the thermal depopulation of the excited Kramer's doublets originated by spin−orbit and low symmetry splitting of $^4T_{1g}$ of the Co^{II} ion.

Considering the complicated structures for **5** and **6**, and the spin−orbit coupling in the Co^{II} atoms, any attempts to fit the $\chi_M T$ data will be unsuccessful.[16−18] Assuming, thus, that the antiferromagnetic coupling inside and between the layers are very small, an attempt has been made to fit the $\chi_M T$ results with the magnetic formula for a mononuclear Co^{II} complex, calculating the λ value (spin−orbit coupling parameter) and the A parameter ($A = 1.5$ in the limit of the small field), and assuming $J = 0$ cm^{-1}, as did by Miller et al. in similar noncoupled complexes.[17] Applying the formula given by Mabbs[16] and Miller,[17] the best fit parameters are $\lambda = -134$ cm^{-1} and $A = 1.30$ for **5**, and $\lambda = -131$ cm^{-1} and $A = 1.45$ for **6**. The λ parameters are close to that expected for an isolated Co^{II} ion (-175 cm^{-1}). The difference indicates the effect of the covalence and the geometrical distortions with regard to regular octahedral Co^{II} complexes. The lack of total coincidence in the shape of these curves (Figure 11) indicates either some amount of weak magnetic coupling or slightly distorted octahedral geometry in cobalt ions, with is consistent with the crystal structure.

It is also possible to apply another different approach: the degeneracy of the $^4T_{1g}$ ground state of the octahedral Co^{II} ion is removed by the action of axial and rhombic distortions of the crystal field, as well as by spin−orbit coupling. The overall effect of low-symmetry crystal field components and spin−orbit coupling produces up to six Kramer's doublets and results in an strongly anisotropic doublet ground state. Thus, at low temperature (<30 K), Co^{II} systems may be described as having an effective spin of $S = {}^1/_2$ with large anisotropy. As a consequence, the assumption of axial J ($J_x = J_y$, J_z) and g_{Co} ($g_x = g_y$, g_z) must be used.[19] With this hypothesis in mind and assuming that $J = 0$, we have carried out a full diagonalization calculation of the magnetization data, considering axial anisotropy of g.[20] The best fit values are as follows: $g_{\parallel} = 5.8$ and $g_{\perp} = 2.4$ for **5** and $g_{\parallel} = 5.5$ and $g_{\perp} = 2.8$ for **6** (see Figures 11a,b, inset). These g values perfectly agree with those reported in the literature for axially distorted Co^{II} systems.[21]

Conclusion

Six new Cu^{II}, Cd^{II}, and Co^{II} coordination polymers based on the organic ligands 2,5-bis(4-pyridyl)-1,3,4-thiadiazole (**L^1**) and 2,5-bis(3-pyridyl)-1,3,4-oxadiazole (**L^3**) have been prepared and structurally characterized by X-ray diffraction analysis. In all these polymers, the ligand takes the bidentate bridging mode when binding to the metal center, and the oxadiazole or thiadiazole nitrogen donors are not involved in the coordination. The interesting porous natures of two 3-D networks **3** and **4** have been investigated by TGA and XPRD techniques. The results demonstrate the framework is retained for complex **3**, and for **4**, the framework is changed but remains regular, after the removal of the guest molecules. Both complexes **3** and **4** may be used to generate new porous materials. A very strong antiferromagnetic coupling is involved in the $[Cu_2(OAc)_4]$ dimeric unit of **1**, and for the other complexes, very weak antiferromagnetic interactions are found due to the long distances of the **L^1** ligands which bridge the Cu^{II} or Co^{II} ions. The coordination chemistry of other type of angular oxadiazole or thiadiazole-containing building blocks is under way in our lab.

Acknowledgment. This work was financially supported by the Outstanding Youth Foundation of NSFC (No. 20225101) and the Spanish government (Grant BQU2000-0791).

Supporting Information Available: X-ray crystallographic data in CIF format for complexes **1**−**6**. This material is available free of charge via the Internet at http://pubs.acs.org.

IC034999D

(15) Antolini, L.; Fabretti, A. C.; Gatteschi, D.; Giusti, A.; Sessoli, R. *Inorg. Chem.* **1991**, *30*, 4858.
(16) Mabbs, F. E.; Machin, D. J. *Magnetism and Transition Metal Complexes*; Chapman and Hall: London, 1973.
(17) Raebiger, J. W.; Manson, J. L.; Sommer, R. D.; Geiser, U.; Rheingold, A. L.; Miller, J. S. *Inorg. Chem.* **2001**, *40*, 2578.
(18) Rizzi, A. C.; Brondino, C. D.; Calvo, R.; Baggio, R.; Garland, M. T.; Rapp, R. E. *Inorg. Chem.* **2003**, *42*, 4409.
(19) Caneschi, A.; Dei, A.; Gatteschi, D.; Tangoulis, V. *Inorg. Chem.* **2002**, *41*, 3508.
(20) The full-diagonalization program was supplied by Prof. Dante Gatteschi (University of Firenze, Italy) and Prof. Vassilis Tangoulis (University of Patras, Greece).
(21) (a) de Munno, G.; Julve, M.; Lloret, F.; Faus, J.; Caneschi, A. *J. Chem. Soc., Dalton Trans*. **1994**, 1175. (b) Hossain, M. J.; Yamasaki, M.; Mikuriya, M.; Kuribayashi, A.; Sakiyama, H. *Inorg. Chem*. **2002**, *41*, 4058. (c) Andres, H.; Clemente-Juan, J. M.; Aebersold, M.; Güdel, H.-U.; Borrás-Almenar, J. J.; Gaita, A.; Coronado, E.; Büttner, H.; Janssen, S. *Inorg. Chem.* **2001**, *40*, 1943. (d) Andres, H.; Clemente-Juan, J. M.; Aebersold, M.; Güdel, H.-U.; Coronado, E.; Büttner, H.; Kearly, G.; Melero, J.; Burriel, R. *J. Am. Chem. Soc*. **1999**, *121*, 10028. (e) Spasojevic, V.; Kusigerski, V.; Sovilj, S. P.; Mrozinski, J.; *J. Magn. Magn. Mater*. **2000**, *219*, 269. (f) Casañ-Pastor, N.; Bas-Serra, J.; Coronado, E.; Pourroy, G.; Baker, L. C. W. *J. Am. Chem. Soc*. **1992**, *114*, 10380.